ARTICLE

Self-Assembly of Silver−Aminosilica Nanocomposites through Silver Nanoparticle Fusion on Hydrophobic Surfaces

Yong-Jae Choi and Tzy-Jiun M. Luo*

Department of Materials Science and Engineering, North Carolina State University, Raleigh, North Carolina 27695

ABSTRACT Silver-nanoparticle-embedded aminosilica colloids synthesized via aminosilane-induced spontaneous reduction reaction exhibit selective adhesion properties on hydrophobic surfaces and have been utilized as a simple and one-step procedure to create patterned nanocomposite film with silver to aminosilica mole ratio at 0.9:1. Substrates that enable self-assembly of the colloids include silicon wafer, polydimethylsiloxane, and microscope slide, where patterns of hydrophilic surface were either created using oxygen plasma treatment or stamped with chemical ink using microcontact printing. Upon substrates being immersed in a solution containing silver-aminosilica colloids, particles attach to hydrophobic surfaces and continuously self-assemble onto the deposited film, allowing us to fabricate nanocomposite patterns with controllable thickness (~200 nm).

KEYWORDS: nanocomposite • sol−gel • silver nanoparticle • self-assembly • hydrophobicity • aminosilane

INTRODUCTION

Fabrication of nanocomposites (1, 2) based on metallic nanoparticles with well-defined dimensions and structures is the important step toward utilization of their unique properties in sensors (3), electrodes (4), biosensors (5−7), and optical application (8−11). Among many patterning techniques (12), the bottom-up approach such as self-assembly through controlled surface chemistry or geometries has been the focus of studies. The motive is that the ability to perform self-assembly processes within predefined area promises the arrangement of nanoscale building blocks with a nanometer precision on a large-scale surface. Because nanocomposites contain more than one component (e.g., silica matrix and metallic nanoparticles), fabrication and patterning of nanocomposites may involve more than one step. For example, patterning of silica film itself can be carried out by depositing silane chemical ink using microcontact printing (13, 14), nanoimprint (15), lift-off of sol−gel layer on microcontact printed monolayer (16), or laser pulse to create sol−gel structures (17). Formation of sol−gel layers can be achieved through self-assembly of surface-bound silane (18), or bioinspired and solution deposition techniques (19, 20). Synthesis or immobilization of metallic nanoparticles in nanocomposite can be carried out using bioinspired approaches (21, 22), synthesized through reductive hydride terminal groups (23), immobilized using polyelectrolytes (24), thermal treatment (25), radiation (26), or spontaneous reduction within silica matrix (27, 28). Fabrication of silica matrix that contains metallic nanoparticles can be performed after synthesis of nanoparticles, examples are direct nanoparticle encapsulation (29, 30), and self-assembly of silica coated nanoparticles (31, 32). Alternatively, formation of nanocomposites as a whole has also been demonstrated using electrochemical codeposition (33), layer-by-layer deposition (34), plasma deposition (35), and radiation (36).

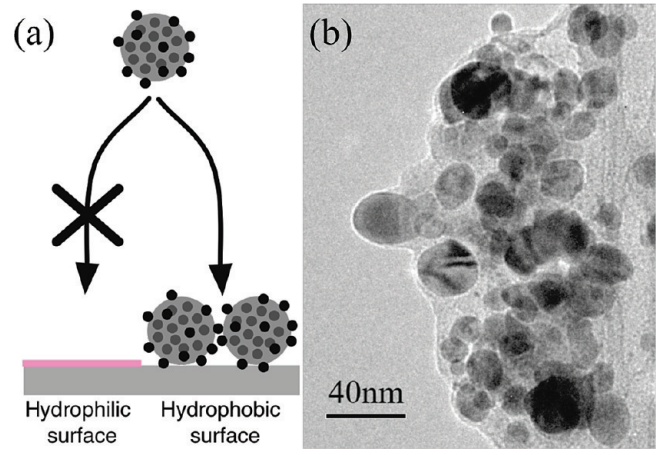

FIGURE 1. (a) Aminosilica colloids containing silver nanoparticles show selective surface adhesion properties. Adhesion results from the binding of the silver nanoparticles to the substrate as well as adhesion of silver nanoparticles occur between two adjacent colloids. (b) The TEM image shows the nanocomposite colloid consists of silver nanoparticles (average diameter is 16 nm).

In this paper, we demonstrate a simple and one-step process to self-assemble nanocomposite colloids into patterns of silver−aminosilica films on various substrates with film thickness controllable by the reaction time. The formation of 3D nanocomposite can be achieved when aminosilica colloids that contain silver nanoparticles are synthesized using room-temperature spontaneous reduction reaction (28), and the colloids show preferential adhesion to hydrophobic areas (Figure 1a). This reduction reaction was carried out by aminosilica precursor, bis[3-(trimethoxysilyl)propyl]-ethylenediamine (enTMOS) (37), also known as an aminosi-

* Corresponding author.
Received for review August 6, 2009 and accepted November 30, 2009
DOI: 10.1021/am900524j

Published on Web 12/11/2009

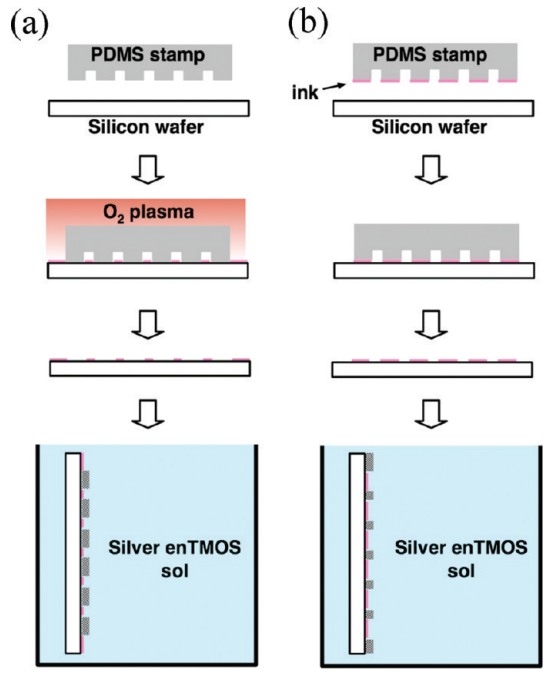

FIGURE 2. Two procedures have been employed to produce modified surface on selective area prior to performing self-assembly in silver enTMOS sol. (a) First approach utilized a PDMS stamp and oxygen plasma to create patterns of treated surface on the substrate. (b) Second method used the PDMS stamp to print a layer of hydrophilic chemical ink through microcontact printing. Two procedures produced films of opposite patterns when the same PDMS stamp is used.

lane. The amino groups of enTMOS serve as both reducing agents and silver ion coordinating sites, while at the same time undergoing sol–gel reaction by reacting with water and forming aminosilica colloids along with silver nanoparticles. (Figure 1b). Substrates that promote self-assembly of nanocomposites include silicon wafer, polydimethylsiloxane (PDMS), and microscope slide. Patterns of hydrophilic regions on the substrates were created using two soft-lithography techniques (38), then the nanocomposite films were created by immersing the substrates into the colloidal solutions (Figure 2). We have found that silver-embedded silica colloids when synthesized under 1:2 mol ratio (silver: aminosilane) exhibit optimal surface selectivity, and their self-assembly can be performed on patterned surfaces with resulting film thickness as the function of reaction time.

MATERIALS AND METHODS

Preparation of Silver enTMOS Sol. All solvents used in the following experiments were ACS grade methanol and purchased from Aldrich Chemical Co. Aminosilane, bis[3-(trimethoxysilyl)-propyl]ethylenediamine (enTMOS), was purchased from Gelest Inc. In general, spontaneous reduction of silver was carried out by mixing 0.1 M silver nitrate and enTMOS stock solutions to result in silver sol suspension according to the previously described procedure (28). Here, methanol solutions containing 80 mM silver nitrate and enTMOS at a desired mole ratio were prepared at 25 °C in a controlled 45% humidity environment prior to the self-assembly experiment, and then the solutions were maintained in a sealed environment at all times to avoid solvent evaporation. Depending on the mole ratios, solutions started to change color within minutes of preparation and their completion time was monitored using UV–vis spectroscopy.

Substrate Preparation. Unless stated otherwise, deposition of silver–aminosilica colloids was performed on silicon wafers. All wafers were cleaned with acetone, sonicated in methanol bath for 10 min, and then rinsed with deionized water. Once the surface was dried under a stream of compressed air, each wafer was surface-treated to create patterns of monolayer using one of the following two methods. First method utilized oxygen plasma to create a layer of –OH terminal groups at the surface: A PDMS stamp with parallel strip patterns that were fabricated according to the procedure described in the literature (39) was placed on top of the wafer, then the surface was plasma-treated for 3 min in a plasma cleaner (model PDC-001, Harrick Plasma). The PDMS stamp has open channels allowing plasma gas to diffuse through and react to uncovered area (Figure 2a). The plasma-treated surface became hydrophilic while the area covered by PDMS remained hydrophobic. Second method utilized soft-lithography method (38) to print a monolayer of chemical film on silicon surface. Here, the same PDMS stamp was immersed in a methanol solution containing 1 mM 3-aminopropyltriethoxysilane (APTS), blow-dried, then pressed against the substrate to create a layer of chemical film (Figure 2b). Alternatively, the substrate with microcontact-printed APTS patterns can be further treated in a methanol solution containing 1 mM (tridecafluoro-1,1,2,2-tetrahydrooctyl)trichlorosilane (i.e., fluorosilane) for 5 min followed by rinsing with methanol and below drying. This procedure allows fluorosilane to be deposited on a previously untreated area. Please note that all surface modification did not produce any visible pattern under optical microscope examination.

Self-Assembly of Silver–Aminosilica Colloids. Individual surface-treated substrate was immersed into a microcentrifuge tube at room temperature that contains freshly prepared silver enTMOS sol. All substrates were placed vertically in the solution to avoid nonspecific binding of precipitated particles and allowed to sit for the desired period of time without disturbance. After the desired reaction time was met, substrates were removed, washed, sonicated in methanol for 3 s, and then blow-dried under a stream of compressed air.

Atomic Force Microscopy. All AFM images were taken on Caliber atomic force microscope (Veeco Inc.) using silicon nanoprobe cantilevers as scanning probes. The noncontact scanning mode (acoustic tapping mode) was used for all measurements in order to avoid surface alteration during the scanning. The tapping amplitude of cantilever was adjusted to 4.5 V prior to sample engagement. Images were measured at a voltage set point of 2.8 V with a scan rate of 0.5–1 Hz. To avoid image distortion, scanning were carried out with active closed-loop on all X, Y, and Z axes. All height mode images reported here were processed using 2D flattening and histogram optimization. To measure the film thickness, we flattened AFM images at the edge of self-assembled films to the silicon wafer substrate; the average height of the self-assembled films was calculated by subtracting the average height of wafer surface from that of film using the roughness function under the surface analysis tool of SPM analysis software.

SEM and TEM Characterization. Scanning electron microscopy images were taken using Hitachi S3200 SEM. The silicon wafer coated with self-assembled film was imaged without sputtering additional metallic coating. The Oxford Isis energy dispersive X-ray spectrometer system attached on the SEM was used to identify the characteristic X-ray emission of elements at specific surface areas with an accelerated voltage at 10 kV.

A gold TEM grid with lacey carbon film was immersed for 30 min in a silver-enTMOS sol containing a 1:2 mol ratio (Ag^+:enTMOS). After being removed from solution, the sample was rinsed with methanol and then dried in the air. The image was taken on Hitachi S3200 and JEOL 2000FX transmission electron microscope with an accelerated voltage of 200 kV.

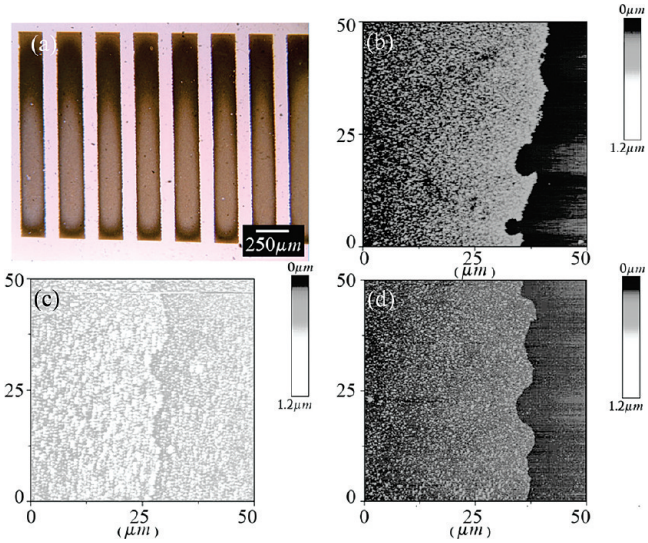

FIGURE 3. (a) Photo of the self-assembled film on silicon wafer surface, where strip pattern of brownish substance (200 μm wide with a 100 μm spacing) was observed after immersing the wafer in a 1:2 solution (Ag^+:enTMOS) for 24 h. The surfaces that have been exposed to oxygen plasma were not covered by the film. AFM images (50 × 50 μm) at the edge of the film show selectivity of assembly on two surfaces after immersing in solutions for 24 h that contain (b) 1:2, (c) 1:1, and (d) 3:1 mol ratios (Ag^+:enTMOS). Optimal selectivity was observed when the mole ratio was 1:2.

RESULTS AND DISCUSSION

The stability of silver nanoparticle embedded colloids synthesized through spontaneous reduction reaction (28) were found to be dependent on the mole ratios of silver and aminosilane. A more stable silver sol was obtained when silver to enTMOS mole ratio was 1:3−1:4, whereas less concentrated enTMOS such as 1:1 ratio resulted in aggregates and deposited on the surface of the container (see the Supporting Information, Figure S1). The stable sol was a clear and light yellow solution that did not deposit at the container wall in 24 h after mixing; on the contrary, solutions of 1:2 mol ratio turned deep brownish color and rapidly deposited a layer of silver coating on the container wall. Reaction kinetics were examined using UV−vis spectroscopy (see Figure S2 in the Supporting Information), which shows that the wavelength of peak absorbance for all solutions was 416−425 nm. Solutions exhibited blue shift to 410−412 nm 24 h after the reaction, which indicates that the silver nanoparticles of smaller size had been produced over time from 20 to 6 nm (40, 41). We found that concentrated enTMOS solution (e.g., Ag^+:enTMOS = 1:3 and 1:4) did not accelerate the reduction reaction, which is due to the higher stoichiometric number of amino groups vs silver ions that inhibits the formation of silver nanoparticles. Less-concentrated enTMOS (Ag^+:enTMOS = 2:1 and 3:1) means fewer reducing agents, but more unprotected silver nanoparticles results in the formation of aggregates and precipitates. The combination of these two effects explains why the mole ratio 1:2 exhibits the maximum kinetics.

Self-assembly experiments in solutions of various mole ratios were first carried out on silicon wafers, where the area of the strip pattern had been treated with oxygen plasma. Figure 3a shows the resulting film after immersing the wafer in a 1:2 ratio solution for 7 days. The area treated with oxygen plasma are not covered by the film. On the contrary, the untreated area steadily grew a layer of brownish film. Selectivity of particle adhesion between treated and untreated surfaces was found to be critically dependent on the mole ratio of silver and enTMOS, which was revealed by examining the edge of the self-assembled film grown for 24 h. In a 1:2 solution, plasma-treated surfaces showed little to no adsorption of particles, whereas the untreated surfaces were completely covered by the film (Figure 3b). AFM images show that the film consists of particles with average diameter of ∼61 nm. When mole ratio was 1:1, the result showed poor selectivity as can be seen at the boundary of two surfaces (Figure 3c), where both surfaces were coated with a layer of particles. Solution of 3:1 ratio resulted in unstable colloids and a thin layer of particles were also observed on both regions (Figure 3d). Particle size at the deposited area is estimated to be 71 nm in diameter, which is larger than that in 1:2 solution. This is possibly due to fewer enTMOS in the solution acting as silver capping agents. These images show that the selectivity of nanocomposite colloids prepared by 1:2 mol ratio solutions is optimal, whereas a 1:1 solution does not exhibit acceptable selectivity. Therefore, a 1:2 solution was chosen for the following self-assembly experiments.

In addition to surface selectivity, silver−aminosilica colloids from 1:2 solution were also found to continuously self-assemble on the deposited film, forming a thicker layer. Figure 4 shows the thickness of the deposited layer vs reaction time. Thickness of the film in the same batch of the solution was 110 nm at 12 h, 133 nm at 24 h, 137 nm at 48 h, then 209 nm at 168 h. The estimated deposition rate was 5 nm/hour in the first 24 h. These results prove that the resistance to surface adhesion remained effective for at least 7 days after merely 3 min of plasma treatment. SEM images on the boundary of a self-assembled film after growing for 24 h are shown in Figure 5a, where a protruded silver−aminosilica composited layer is observed and the hydrophilic area not covered by the film is. The film is composed of particles as shown on the AFM images but some particles appear to be brighter on the SEM image (Figure 5b). The energy-dispersive X-ray spectroscopy (EDX) shows that the brighter particles contain higher silver contents (Figure 5c). Spectrum indicates that Si, Ag, and C elements are present in the composite film. Silver and carbon mole ratio was determined to be 0.33:1, which is equal to ∼2.6:1 ratio of Ag and enTMOS. Particles that appear dark on SEM image are low in silver content (Figure 5d), which is ∼0.9:1 (Ag:enTMOS). Because two EDX spectra were taken under comparable beam size, an equal intensity of C signal indicates similar enTMOS amounts in these two regions. The particles containing the higher Ag amount are due to aggregation/fusion of silver nanoparticles. Silver nanoparticles in the low Ag region were also confirmed by the TEM studies (see the Supporting Information, Figure S3). We have also examined the EDX spectra of nanocomposite films from solutions of different mole ratio and found that the ratio of

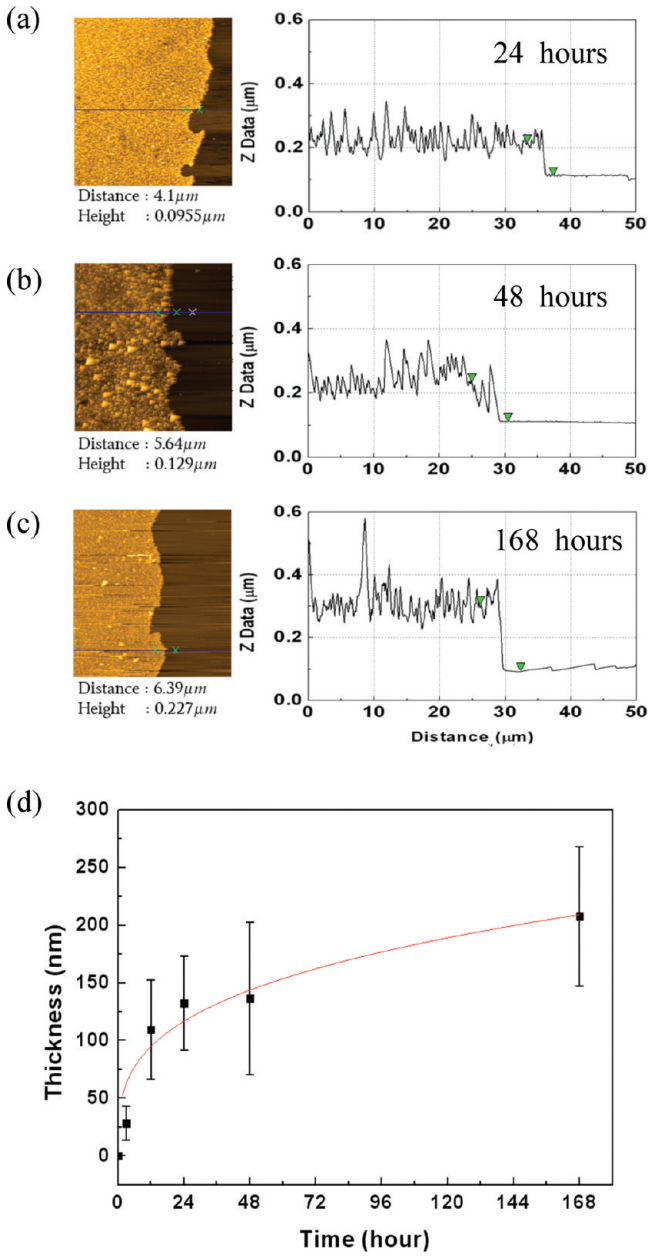

FIGURE 4. (a–c) AFM images (50 × 50 μm) at the edge of self-assembled films synthesized under various reaction times. The height-profile maps across both treated and untreated regions reveal well-defined cutoff boundaries on all samples. (d) Thickness of the film vs reaction time showing the deposition can be continuously performed in solutions for 168 h (7 days). The thickness of the film was measured at the boundary of self-assembled pattern by comparing the average height of both regions.

nanocomposites are 0.8:1–0.9:1 with silver aggregates can be as high as 4:1–5.5:1 ratios. The composition of nanocomposite films is constant regardless of the mole ratio of the solutions, whereas more enTMOS such as 1:2 (Ag^+:enTMOS) results in smaller size colloids with fewer large aggregates. Both TEM and EDX studies prove that the deposited layer is nanocomposite in nature, which contains silver nanoparticles within aminosilica layer.

Two depositing mechanisms are proposed here: growth of silver-aminosilica colloids and self-assembly of colloids onto the deposited layer. The increase in colloidal size was identified using high-resolution AFM, which reveals that the growth of individual particle at the surface is through the aggregation of smaller silver-aminosilica colloids as can be seen in Figure 6a–d. The average particle sizes of the self-assembled film on day 1 and day 2 are estimated to be 277 and 264 nm, with primary particle size for day 1, 2, and 7 being 61, 70, and 22 nm, respectively. The AFM image of the film after 7 days of growth also confirms that there exist smaller diameter colloids on the surface of film (Figure 6d). This is probably due to the smaller size of silver nanoparticles being continuously produced at the later stage of the reaction. Considering the primary size of silver nanoparticles is around 6–20 nm as indicated on UV–vis spectroscopy (see Figure S2 in the Supporting Information) and TEM (Figure 1 and Figure S3 in the Supporting Information), which is significantly smaller than that of the colloids, we speculate that silver nanoparticles at the surface of aminosilica colloids are critical in both substrate adhesion and self-assembly. This also explains why large silver aggregates appear on all SEM images. We also identified the controlled environment at minimum 45% humidity is necessary for preparing solutions that exhibit self-assembly property, because the colloidal structure of aminosilica is formed under this condition. Self-assembly of nanocomposite colloids on the existing film can be explained using Ostwald ripening (42). Growth of silver–aminosilica colloids are made possible with formation of Si–O–Si bond and fusion of silver nanoparticles at the colloidal surface, both of which in combination are also responsible for selective surface adhesion, increase in colloidal diameter, and growth of film thickness. In addition, unprotected silver nanoparticles, once attached to surface or substrates, are considered adhesive and prone to fusion as reported by the literatures (43–45), which is due to the presence of anisotropic cohesive force when only one side of the nanoparticle is bounded (46).

The surface selectivity is the result of balancing adhesion and repulsive forces between colloids and the substrate. Because aminosilane at lower concentration is not an effective capping agent for silver nanoparticles, uncapped silver nanoparticles tend to adhere to surfaces. As shown in Figure 3c, colloids produced from 1:1 solutions contain fewer aminosilica components, and therefore poor selectivity was observed. On the contrary, pure aminosilica colloids show poor adhesion to hydrophilic surfaces because of the repulsive force between silanol-terminated surfaces (Si–OH) and the solvent cushion layer at the hydrophilic surfaces (47). Intrinsic positive charges on the surfaces of aminosilica colloids should also prevent aggregation of colloids, as is evidenced by the zeta potential measurement of stable aminosilica colloids over ~30 mV. Therefore, colloids from the solutions containing a high concentration of aminosilane (e.g., 1:3) exhibit a slower deposition rate. We have also observed larger silver aggregates from solutions containing less concentrated aminosilane (see Figure S4 in the Supporting Information), indicating stronger silver aggregation.

Selective self-assembly was further demonstrated on polydimethylsiloxane (PDMS) and microscope glass slide (Figure 7a,b). Patterns were created following the first

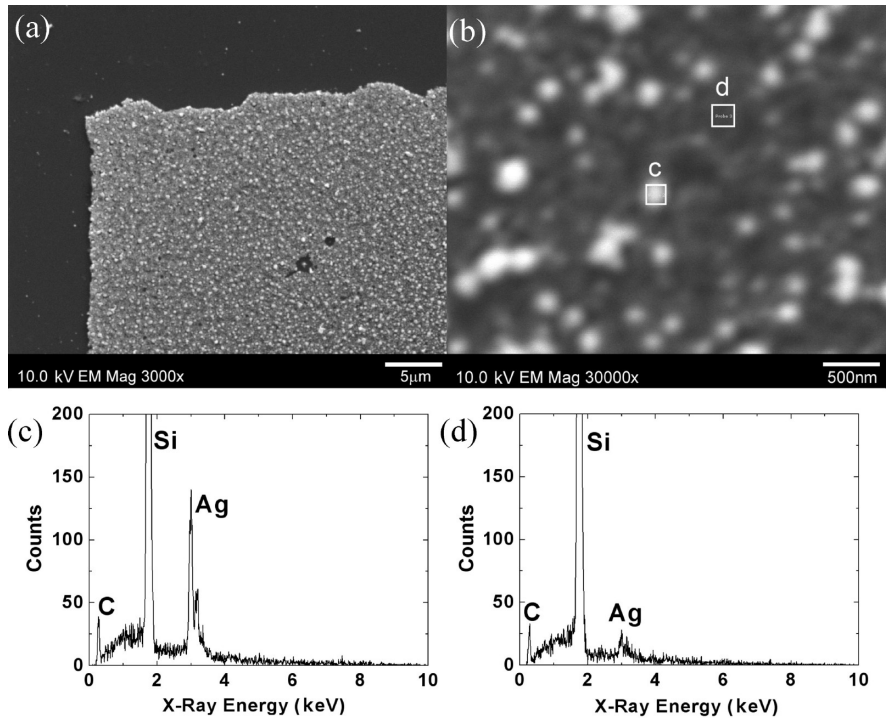

FIGURE 5. (a) SEM micrograph at the edge of silver-aminosilica nanocomposite film (thickness ~133 nm) that has been self-assembled on wafer surface for 24 h in a 1:2 methanol solution (Ag^{+}:enTMOS). The area that is not covered by the film was previously treated with oxygen plasma. (b) SEM image of the same film at 30 000× magnification. Film is composed of colloidal particles with some particles appear brighter on the image. Energy-dispersive X-ray spectra (EDX) of (c) bright and (d) dark regions as indicated on SEM image show that the film contains both silver and carbon elements with brighter particles containing more silver content.

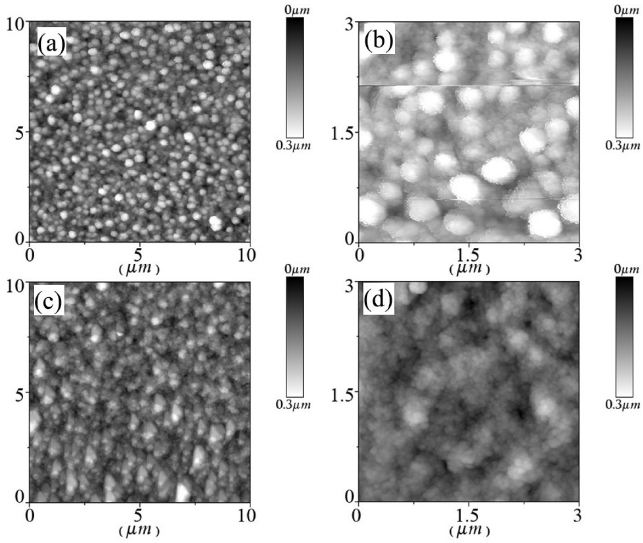

FIGURE 6. (a) AFM image (10 × 10 μm) of a self-assembled film fabricated in 1:2 solution for 24 h. (b) High resolution AFM image (3 × 3 μm) shows that the film consists of large colloidal particles (diameter ~277 nm). (c) AFM image (10 × 10 μm) of a self-assembled film that has been grown in solution for 7 days. (d) Surface of the film at 3 × 3 μm size reveals the surface consists of small diameter particles (diameter ~22 nm).

method described in the experimental section. Both substrates were hydrophobic, which attracted colloids and formed a self-assembled layer. A similar result was also observed on silicon surface, where patterns of a monolayer of 3-aminopropyltriethoxysilane (APTS) were created using microcontact printing (Figure 7c). Photos show that the APTS-coated areas on silicon wafer are not covered by the nanocomposite film, whereas the untreated surfaces are covered by a layer of the film. Selectivity of deposition was also confirmed on the APTS-modified silicon wafer where previously unmodified areas had been surface-treated in a fluorosilane solution. Nanocomposite films in Figure 7d appear to be thicker and darker on the fluorosilane-treated area compared to the film grown on the unmodified surface area (Figure 7c), proving that the more hydrophobic surface exhibits enhanced adhesion property. Please note that the partial deposition of nanocomposite film on the APTS-coated regions in Figure 7d is due to the formation of fluorosilane monolayer at the defect sites of APTS monolayer that promoted adhesion of the colloids. These results also prove that selective self-assembly of silver−aminosilica nanocomposite can be controlled simply using surface hydrophobicity.

The selectivity of the self-assembly process at the nanometer scale was attempted on the silicon wafer, where the dimensions of strip patterns and the size of silver−aminosilica colloids were on the same order of magnitude. A PDMS replicate stamp with parallel strip patterns was utilized to create parallel hydrophilic area with an individual width at 300 nm. Figure 8a illustrates that silver−aminosilica colloids arranged in parallel strips were successfully self-assembled onto the unmodified areas of silicon wafer after immersing in solution for 24 h. Under high-resolution AFM, it was also observed that strips of silver−aminosilica layer are composed of individual colloid (Figure 8b). AFM images show that the height of an individual particle of the assembled strips is 40−45 nm (Figure 8c), which is approximately equal to the average size of silver−aminosilica particles as previ-

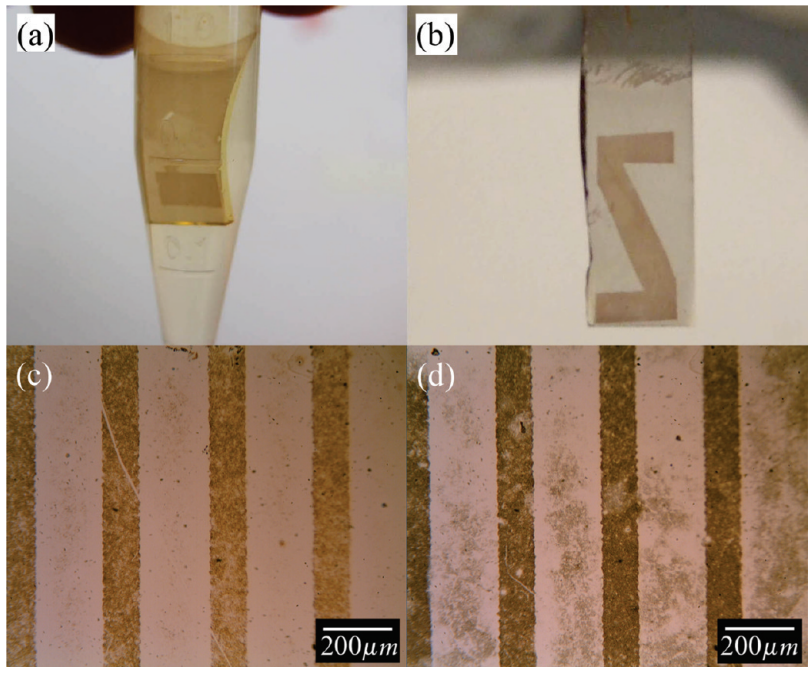

FIGURE 7. Self-assembly of nanocomposite colloids was performed on (a) PDMS, (b) microscope slide, and (c) 3-aminopropyltriethoxysilane (APTS) modified silicon wafer. Each of APTS strip pattern is 100 μm wide and separated by 200 μm spacing, where unmodified areas promote the deposition of nanocomposite. (d) Improved binding of colloids was observed when the silicon wafer was further treated in a fluorosilane solution after APTS pattern was created.

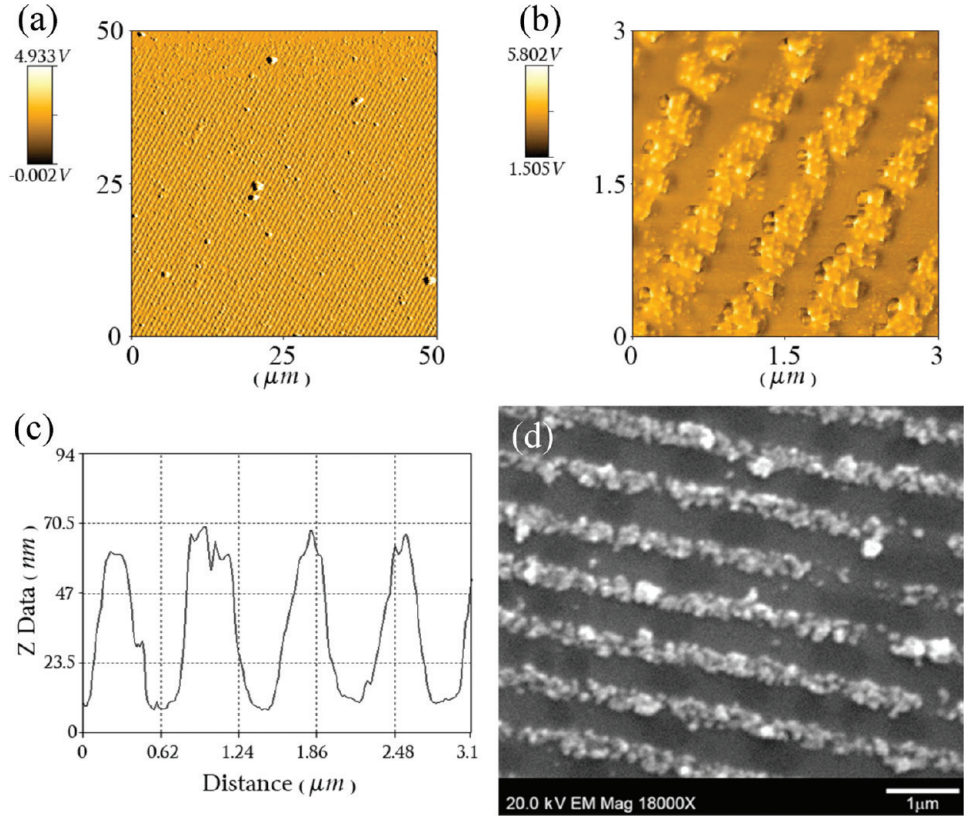

FIGURE 8. (a) AFM image (50 $\times$ 50 μm) of self-assembled nanocomposite strips on silicon wafer (300 nm wide and 400 nm apart). (b) High-resolution AFM image (3 $\times$ 3 μm) shows that the strips consist of colloidal particles. (c) Height profile of the strips shows the average height is $\sim$ 50 nm. (d) SEM image of the nanocomposite strips at 18 000$\times$ magnification confirms that the individual strip consists of individual particles.

ously discussed. SEM reveals that each strip consists of tightly packed particles on the surface (Figure 8d). Results indicate 300 nm wide hydrophobic area attracts only a monolayer of colloids. We observed that the maximum height of some strip can reached $\sim$100 nm when large particles were on top of the strip pattern as shown in Figure

8d, indicating that self-assembly of colloids also occurs through stacking to the existing nanocomposite strips.

CONCLUSION

Aminosilica colloids containing silver nanoparticles synthesized from solution of silver ion and aminosilane at a 1:2 mol ratio were found to selectively adhere to hydrophobic surfaces and have been utilized to create 3D nanocomposite structures on silicon wafer, PDMS, and microscope glass slide. Colloids do not bind to hydrophilic regions on the substrates but continuously self-assemble on the surface of existing film with an average growth rate at 5 nm/h within the first 24 h. Successful demonstration of self-assembly of silver−aminosilica colloids on nanoscale patterns suggests that it is possible to create on a large scale the nanocomposite sol−gel structures with feature size controllable at the nanometer scale.

Acknowledgment. The authors acknowledge the financial support of NCSU Faculty Research and Professional Development Fund and the Oak Ridge Associated Universities for partial support of this research, and Chi-Kai Chiu for performing TEM measurements.

Supporting Information Available: Figures S1−S4 include photos of samples prepared under different mole ratios, kinetics measurements of the solutions using UV−vis spectroscopy, and TEM and SEM images of the deposited films (PDF). This material is available free of charge via the Internet at http://pubs.acs.org.

REFERENCES AND NOTES

(1) Komarneni, S. *J. Mater. Chem.* **1992**, *2*, 1219–1230.
(2) Armelao, L.; Barreca, D.; Bottaro, G.; Gasparotto, A.; Gross, S.; Maragno, C.; Tondello, E. *Coord. Chem. Rev.* **2006**, *250*, 1294–1314.
(3) Mizsei, J.; Sipila, P.; Lantto, V. *Sens. Actuators, B* **1998**, *47*, 139–144.
(4) Wang, J.; Pamidi, P. V. A. *Anal. Chem.* **1997**, *69*, 4490–4494.
(5) Bharathi, S.; Lev, O. *Anal. Commun.* **1998**, *35*, 29–31.
(6) Jia, J. B.; Wang, B. Q.; Wu, A. G.; Cheng, G. J.; Li, Z.; Dong, S. *J. Anal. Chem.* **2002**, *74*, 2217–2223.
(7) Wu, Z. S.; Li, J. S.; Luo, M. H.; Shen, G. L.; Yu, R. Q. *Anal. Chim. Acta* **2005**, *528*, 235–242.
(8) Yazawa, T.; Kadono, K.; Tanaka, H.; Sakaguchi, T.; Tsubota, S.; Kuraoka, K.; Miya, M.; Wang, D. X. *J. Non-Cryst. Solids* **1994**, *170*, 105–108.
(9) Akbarian, F.; Dunn, B. S.; Zink, J. I. *J. Phys. Chem.* **1995**, *99*, 3892–3894.
(10) Zhang, R. J.; Chen, L. Y.; Wang, S. Y.; Qian, D. L.; Zheng, Y. X.; Zhou, S. M.; Yang, Y. M.; Dai, N.; Wang, Y.; Zhang, X. X.; Yan, X. *J. Appl. Phys.* **1999**, *85*, 5118–5120.
(11) Sanchez, C.; Lebeau, B.; Chaput, F.; Boilot, J. P. *Adv. Mater.* **2003**, *15*, 1969–1994.
(12) Geissler, M.; Xia, Y. N. *Adv. Mater.* **2004**, *16*, 1249–1269.
(13) Jeon, N. L.; Finnie, K.; Branshaw, K.; Nuzzo, R. G. *Langmuir* **1997**, *13*, 3382–3391.
(14) Pompe, T.; Fery, A.; Herminghaus, S.; Kriele, A.; Lorenz, H.; Kotthaus, J. P. *Langmuir* **1999**, *15*, 2398–2401.
(15) Peroz, C.; Chauveau, V.; Barthel, E.; Sondergard, E. *Adv. Mater.* **2009**, *21*, 555–558.
(16) Payne, D. A.; Clem, P. G. *J. Electroceram.* **1999**, *3*, 163–172.
(17) Passinger, S.; Saifullah, M. S. M.; Reinhardt, C.; Subramanian, K. R. V.; Chichkov, B. N.; Welland, M. E. *Adv. Mater.* **2007**, *19*, 1218–1221.
(18) Wang, J.; Pamidi, P. V. A.; Zanette, D. R. *J. Am. Chem. Soc.* **1998**, *120*, 5852–5853.
(19) Coradin, T.; Lopez, P. J. *Chembiochem* **2003**, *4*, 251–259.
(20) Gao, Y. F.; Koumoto, K. *Cryst. Growth Des.* **2005**, *5*, 1983–2017.
(21) Hall, S. R.; Shenton, W.; Engelhardt, H.; Mann, S. *Chemphyschem* **2001**, *2*, 184–186.
(22) Kharlampieva, E.; Slocik, J. M.; Tsukruk, T.; Naik, R. R.; Tsukruk, V. V. *Chem. Mater.* **2008**, *20*, 5822–5831.
(23) Porter, L. A.; Choi, H. C.; Schmeltzer, J. M.; Ribbe, A. E.; Elliott, L. C. C.; Buriak, J. M. *Nano Lett.* **2002**, *2*, 1369–1372.
(24) Wei, H.; Li, J.; Wang, Y. L.; Wang, E. K. *Nanotechnology* **2007**, 18.
(25) Carpenter, J. P.; Lukehart, C. M.; Milne, S. B.; Henderson, D. O.; Mu, R.; Stock, S. R. *Chem. Mater.* **1997**, *9*, 3164–3170.
(26) Hornebecq, V.; Antonietti, M.; Cardinal, T.; Treguer-Delapierre, M. *Chem. Mater.* **2003**, *15*, 1993–1999.
(27) Wu, P. W.; Dunn, B.; Doan, V.; Schwartz, B. J.; Yablonovitch, E.; Yamane, M. *J. Sol−Gel Sci. Technol.* **2000**, *19*, 249–252.
(28) Choi, Y.-J.; Huh, U.; Luo, T.-J. M. *J. Sol−Gel Sci. Technol.* **2009**, *51*, 124–132.
(29) Epifani, M.; Giannini, C.; Tapfer, L.; Vasanelli, L. *J. Am. Ceram. Soc.* **2000**, *83*, 2385–2393.
(30) Kobayashi, Y.; Correa-Duarte, M. A.; Liz-Marzan, L. M. *Langmuir* **2001**, *17*, 6375–6379.
(31) Lu, Y.; Yin, Y. D.; Li, Z. Y.; Xia, Y. A. *Nano Lett.* **2002**, *2*, 785–788.
(32) Fan, H. Y.; Wright, A.; Gabaldon, J.; Rodriguez, A.; Brinker, C. J.; Jiang, Y. B. *Adv. Funct. Mater.* **2006**, *16*, 891–895.
(33) Toledano, R.; Shacham, R.; Avnir, D.; Mandler, D. *Chem. Mater.* **2008**, *20*, 4276–4283.
(34) Tseng, J. Y.; Lin, M. H.; Chau, L. K. *Colloids Surf., A* **2001**, *182*, 239–245.
(35) Dalacu, D.; Martinu, L. *J. Appl. Phys.* **2000**, *87*, 228–235.
(36) Gacoin, T.; Chaput, F.; Boilot, J. P.; Jaskierowicz, G. *Chem. Mater.* **1993**, *5*, 1150–1156.
(37) Rao, M. S.; Dubenko, I. S.; Roy, S.; Ali, N.; Dave, B. C. *J. Am. Chem. Soc.* **2001**, *123*, 1511–1512.
(38) Xia, Y. N.; Whitesides, G. M. *Annu. Rev. Mater. Sci.* **1998**, *28*, 153–184.
(39) Xia, Y.; Kim, E.; Whitesides, G. M. *J. Electrochem. Soc.* **1996**, *143*, 1070–1079.
(40) Creighton, J. A.; Eadon, D. G. *J. Chem. Soc., Faraday Trans.* **1991**, *87*, 3881–3891.
(41) Tanahashi, I.; Yoshida, M.; Manabe, Y.; Tohda, T. *J. Mater. Res.* **1995**, *10*, 362–365.
(42) Brinker, C. J.; Scherer, G. W. In *Sol−Gel Science: The Physics and Chemistry of Sol−Gel Processing*, 1st ed.; Academic Press: New York, 1990; pp 97−104.
(43) Li, J.; Lin, Y. Q.; Zhao, B. G. *J. Nanopart. Res.* **2002**, *4*, 345–349.
(44) Yonezawa, T.; Onoue, S. Y.; Kimizuka, N. *Chem. Lett.* **2002**, 1172–1173.
(45) Yonezawa, T.; Onoue, S. Y.; Kimizuka, N. *Chem. Lett.* **2005**, *34*, 1498–1499.
(46) Nanda, K. K.; Maisels, A.; Kruis, F. E.; Fissan, H.; Stappert, S. *Phys. Rev. Lett.* **2003**, *91*, 106102–4.
(47) Besseling, N. A. M. *Langmuir* **1997**, *13*, 2113–2122.

AM900524J